THE JOURNAL OF PHYSICAL CHEMISTRY A

pubs.acs.org/JPCA Article

The Elusive Noncanonical Isomers of Ionized 9-Methyladenine and 2′-Deoxyadenosine

Shu R. Huang, Gabriela Nováková, Aleš Marek,* and František Tureček*

Cite This: J. Phys. Chem. A 2021, 125, 338−348 Read Online

ACCESS | Metrics & More | Article Recommendations | Supporting Information

ABSTRACT: Noncanonical nucleobases and nucleosides represent newly discovered species of relevance for DNA ionization. We report a targeted synthesis of gas-phase 9-methylene(1*H*)adenine cation radical ($\mathbf{2}^{+\cdot}$) as a low-energy isomer of ionized 9-methyladenine. Ion $\mathbf{2}^{+\cdot}$ showed unique collision-induced dissociation and UV−vis photodissociation action spectra that distinguished it from other cation radical isomers. Ab initio energy calculations with coupled cluster theory extrapolated to the complete basis set limit, CCSD(T)/CBS, identified cation radical $\mathbf{2}^{+\cdot}$ as the global energy minimum of the adenine-related $C_6H_7N_5^{+\cdot}$ isomers. The action spectrum of $\mathbf{2}^{+\cdot}$ was assigned on the basis of vibronic absorption spectra that were calculated with time-dependent density functional theory for multiple vibrational configurations of thermal ions. The major dissociation of $\mathbf{2}^{+\cdot}$ proceeded by hydrogen loss that was elucidated by deuterium labeling at the exchangeable N-1 and NH_2 positions and C-8 position and by kinetic analysis. The dissociation involved a reversible rearrangement to intermediate dihydropteridine structures, yielding a protonated aminopteridine as the product, which was identified by multistep UV−vis action spectroscopy. We also report a computational study of related noncanonical isomers of 2′-deoxyadenosine cation radical having the radical defect at C-1′ that were found to be thermodynamically more stable than the canonical isomer in both the gas phase and aqueous solution. The noncanonical isomers were calculated to have extremely low ion−electron recombination energies of 4.42−5.10 eV that would make them dead-end hole traps if produced by DNA ionization.

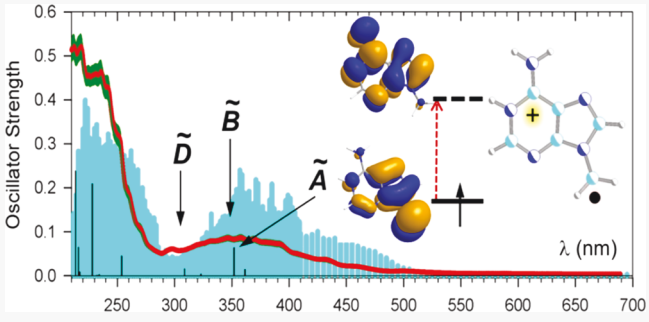

INTRODUCTION

The DNA nucleobases represent chemically stable and biologically conserved heteroaromatic molecules of essential importance for terrestrial life forms. Ionization by high-energy particles or photons disrupts the nucleobase π-electronic system, rendering nucleobase cation radicals susceptible to fast electron- and proton-transfer reactions within DNA or with surrounding molecules. Previous experimental and theoretical investigations of nucleobase cation radicals have largely treated these reactive species within the paradigm of canonical structures produced by electron removal from neutral nucleobases.[1−13] However, this paradigm has been challenged recently by the generation of stable noncanonical isomers of the thymine[14] and 1-methylcytosine[15] cation radicals in the gas phase. Computational energy analysis of the noncanonical cation radicals of both thymine (4-hydroxy-5-methylene-(1,3*H*)pyrimid-2-one)[14,16] and 1-methylcytosine (1-methylene-2-hydroxy-4-aminopyrimidine)[15] revealed that they were substantially more stable than the pertinent canonical forms of oxidized DNA nucleobases. The discovery of noncanonical nucleobase cation radicals has been made possible by a combination of methods of gas-phase ion chemistry to generate such unusual species[17,18] and UV−vis photodissociation (UVPD) action spectroscopy[19−21] to characterize the ions and distinguish them from their canonical isomers and other protomers. Ion action spectroscopy relies on photodissociation of mass-selected gas-phase ions whereby the wavelength-dependent photofragment ion intensities are used to reconstruct the absorption profile of the precursor ion. Several variants of action spectroscopies have been developed working in the infrared or UV−vis regions of the spectrum.[22−24] Multiphoton infrared photodissociation spectroscopy has been the most popular technique for small ions,[25] whereas its applications to strongly hydrogen bonded systems have faced difficulties with band assignment and spectral interpretation.[26,27] UV−vis spectroscopy utilizing valence electron excitation and single-photon dissociation largely avoids such issues and has been shown to provide structural information for larger biomolecular ions that show characteristic absorption bands, such as peptide and oligonucleotide cation radicals.[28−32]

Received: November 15, 2020
Revised: December 7, 2020
Published: December 22, 2020

https://dx.doi.org/10.1021/acs.jpca.0c10293
J. Phys. Chem. A 2021, 125, 338−348

The previously reported noncanonical nucleobase cation radicals have been generated by collision-induced oxidation of nucleobase ligands in metal ternary complexes[17,18] that relied on ion thermodynamics while not allowing one to have a mechanistic control over the produced ion structures.[14,15] We now report a combined experimental and ab initio computational study documenting a specific generation of a stable noncanonical isomer of 9-methyladenine cation radical that we complement with energy analysis of cation radicals of 2′-deoxyadenosine. Purine and pyrimidine nucleobases carrying a methyl group at N-9 or N-1, respectively, which are the linking positions to 2′-deoxyribose in DNA, have often been used as simplified models for nucleosides to limit the number of theoretical protomers while maintaining intact the π-electronic system of the nucleobase.[1,17,18]

Two low-energy noncanonical isomers of 9-methyladenine cation radical ($\mathbf{1}^{+\cdot}$) have recently been identified by ab initio calculations as 9-methylene-(1*H*)adenine ($\mathbf{2}^{+\cdot}$) and 9-methylene-(3*H*)adenine ($\mathbf{3}^{+\cdot}$) (Scheme 1).[33] However, synthetic

Scheme 1. Low-Energy Isomers of 9-Methyladenine Cation Radical

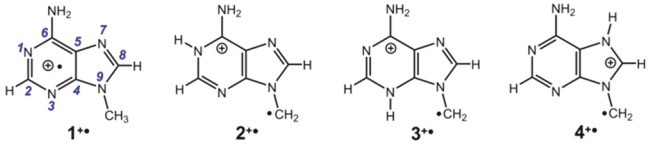

pathways to generating ions $\mathbf{2}^{+\cdot}$ and $\mathbf{3}^{+\cdot}$ have not been established, especially in light of the energy analysis of the potential energy surface that has indicated large energy barriers separating the isomers and precluding unimolecular isomerization.[33] We reasoned that an adenine derivative carrying an N-9 CH_2−X group can be protonated, yielding a stable gas-phase ion in which a labile C−X bond, such as C−I, could be homolytically cleaved upon collisional activation to form a ring-protonated 9-CH_2 radical, such as $\mathbf{2}^{+\cdot}$ (Scheme 2) or its N-3 ($\mathbf{3}^{+\cdot}$) or N-7-protonated tautomers ($\mathbf{4}^{+\cdot}$).

A similar approach has been used by Kenttämaa and coworkers to generate σ-radicals in gas-phase distonic heteroaromatic ions.[34−37] According to our preliminary ab initio and density functional theory (DFT) calculations, thermodynamics favors N-1 in 9-alkyl-substituted adenines as the most basic position, possibly providing a pathway to generating $\mathbf{2}^{+\cdot}$.

EXPERIMENTAL SECTION

Materials. Formaldehyde, adenine, thionylchloride, and deuterated solvents were obtained from Sigma-Aldrich (Milwaukee, WI). Solvents used in synthesis were purchased from Acros Organics (Geel, Belgium) or Penta Chemicals Unlimited (Prague, Czech Republic). *N*-Bromosuccinimide was purchased from Fluka Chemie GmbH (Buchs, Switzerland), and Pd/$CaCO_3$ (5%, type 405) was from Johnson Matthey (Prague, Czech Republic). Reagents and solvents were used without further purification. 9-Iodomethyladenine and [8-D]-9-iodomethyladenine were synthesized according to Scheme 3.

A detailed description of the synthetic procedures and product spectroscopic characterization are provided in the Supporting Information (Schemes S1 and S2).

Methods. ^{1}H and ^{13}C NMR spectra were recorded on a Bruker Avance II spectrometer at 300 and 75 MHz, respectively, at 25 °C. Experiments with tandem mass and photodissociation action spectra were performed on a modified amaZon speed 3D ion trap tandem mass spectrometer (Bruker Daltonik, Bremen, Germany) equipped with an EKSPLA NL301G Nd-YAG laser (Altos Photonics, Bozeman, MT, USA) working at 20 Hz frequency and 3 to 6 ns pulse width, as described in detail previously.[38] Photofragment ion intensities were measured in three sections covering the 210−354, 355−409, and 410−700 nm ranges and normalized to the number of photons per pulse that was determined from laser pulse energy measurements at each experimental wavelength. The action spectra were reproduced on different days and are reported as averages of two measurements. Experiments involving H/D exchange were carried out in D_2O/CD_3CN solution that was used for electrospray ionization. The D content in gas-phase ions was maintained by feeding D_2O solvent vapor into the dry nitrogen stream flushing the enclosed electrospray interface volume. A high-resolution Orbitrap Velos mass spectrometer (Thermo Fisher, San Jose, CA, USA) was used to measure accurate mass-to-charge ratios at a resolving power of 60,000.

Calculations. We used the Gaussian 16 (Revision A03) suite of programs[39] to carry out ab initio and density functional theory (DFT) calculations of ions and neutral molecules of interest. Structures were first optimized using the hybrid B3LYP[40] and CAM-B3LYP[41] functionals and the 6-31+G(d,p) and 6-311+G(2d,p) basis sets, respectively, to obtain a preliminary ranking of the cation radical tautomers. Harmonic frequencies were used to identify local energy minima as having all real frequencies and transition states as having one imaginary frequency. Based on our previous analysis and benchmarking of optimized geometries of nucleobase cation radicals,[15,33] we obtained additional sets of optimized geometries with M06-2X[42] and the 6-31+G(d,p) and 6-311++G(2d,p) basis sets to be used in single-point energy calculations. All these calculations were performed within the spin-unrestricted formalism. Solvation energies were calculated with full gradient optimization by the polarizable continuum model (PCM)[43] and M06-2X/6-311++G(2d,p). Single-point energies were calculated using coupled clusters[44] with single, double, and disconnected triple excitations, CCSD(T),[45] and extrapolated to the complete

Scheme 2. Reaction Sequence Leading to Ion $\mathbf{2}^{+\cdot}$ Involving Electrospray Ionization (ESI) and Collision-Induced Dissociation (CID)

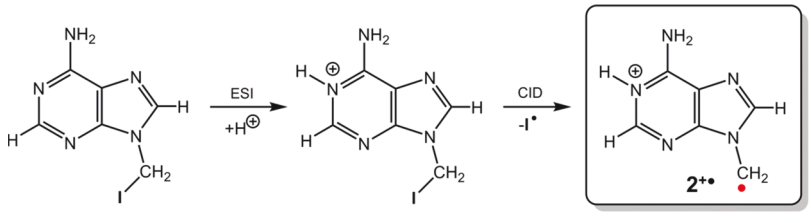

https://dx.doi.org/10.1021/acs.jpca.0c10293
J. Phys. Chem. A 2021, 125, 338−348

Scheme 3. Synthesis of 9-Iodomethyladenine and [8-D]-9-Iodomethyladenine

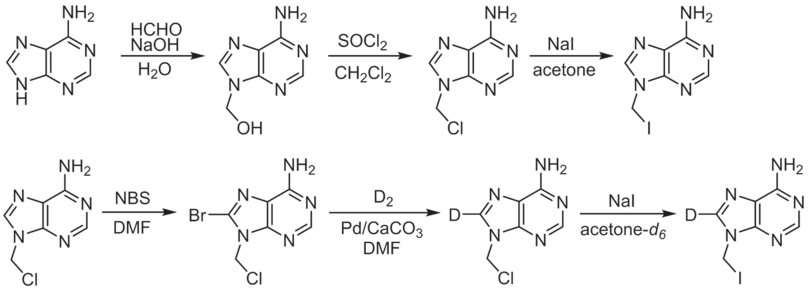

basis set (CBS),[46] providing benchmark relative energies. We used the formula E[CCSD(T)/CBS] ≈ E[CCSD(T)/aug-pVDZ] − E[MP2/aug-pVDZ] + E[HF/aug-pVQZ] + $E_{corr,CBS}$, to extrapolate the basis set and obtain benchmark relative energies. The correlation energy at the complete basis set limit was calculated with least-squares fits to the standard two-parameter formula,[47] $E_{corr,CBS} = \lim(X \rightarrow \infty)E_{corr,X} = E$[HF/aug-cc-pVXZ] − E[MP2/aug-cc-pVXZ] = A + BX^{-3}, where X is the ζ split in the aug-cc-pVXZ basis set.[48] Higher spin states in the UMP2 calculations were treated with the spin projection method[49,50] by spin annihilation that reduced the total spin close to the theoretical value (0.75). Electronic excitations were evaluated using equation-of-motion CCSD (EOM-CCSD) calculations[51] with the 6-31+G(d,p) basis set for 16−18 excited electronic states, covering excitations down to 200 nm for all ions. We used the EOM-CCSD transitions to assign transitions in time-dependent DFT (TD-DFT)[52] calculations that were carried out with M06-2X. We found that 35−40 excited states in adenine and 9-methyladenine cation radicals were sufficient to cover the wavelength range to below 180 nm. The M06-2X TD-DFT calculations with the 6-31+G(d,p) and 6-311++G(2d,p) basis sets gave very similar results in terms of excitation energies and oscillator strength, as reported recently for other nucleobase cation radicals.[15,33] Therefore, the M06-2X/6-31+G(d,p) TD-DFT calculations were used to calculate all vibronic spectra at 310 K. The B3LYP/6-31+G(d,p) normal modes were used to generate Wigner distributions[53,54] of vibrational configurations of the ground electronic state. This was performed with the Newton-X 16 program.[55] The configurations were ordered according to their Boltzmann factors at 310 K, and 300 lowest-energy configurations were selected and submitted to TD-DFT M06-2X/6-31+G(d,p) calculations for 20 excited states to generate the vibronic spectra reported here. To address the dissociation kinetics, we performed Rice−Ramsperger−Kassel−Marcus (RRKM) calculations of rate constants[56] using the QCPE program[57] that was recompiled and run under Windows 7, as described previously.[58] Born−Oppenheimer molecular dynamics (BOMD) trajectories were run with semiempirical all-valence-electron quantum chemistry calculations using the Berendsen thermostat algorithm.[59] Temperature was set at 310 K to approximate the experimental conditions in the ion trap. For each 2′-deoxyadenosine tautomer, several (>5) initial structures were constructed from PM6-optimized adenosine cation radicals with different nucleobase-deoxyribose orientations and ring conformations. These structures were subjected to a preliminary BOMD using PM6[60] that was augmented by including dispersion interactions (D3H4).[61] These calculations were run by MOPAC[62] that was coupled to the Cuby 4 framework.[63,64] Running trajectories with 1 fs steps for 20 ps furnished 20,000 snapshots per each initial structure from which 200 snapshots were extracted at 100 fs intervals. The extracted snapshot structures were fully gradient-optimized with PM6-D3H4 and sorted out by their secondary structural similarities to compact duplicates and reduce the size of the selection. This yielded 10−20 distinct structures whose geometries were fully gradient-optimized by B3LYP and M06-2X/6-31+G(d,p) calculations.

RESULTS AND DISCUSSION

Ion Generation and Spectra. Electrospray ionization of 9-iodomethyladenine generated the protonated ion (m/z 276)

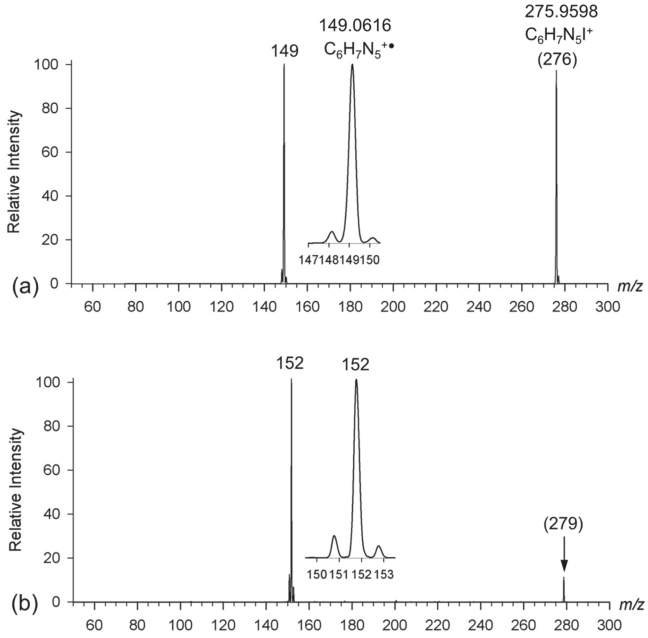

Figure 1. (a, b) CID-MS^2 spectra of (a) protonated 9-iodomethyladenine ion and (b) [D_3]-9-iodomethyladenine ion. Insets show the cation radical peak profiles.

that upon mass isolation and collision-induced dissociation (CID) eliminated iodine, giving rise to the $C_6H_7N_5^{+\cdot}$ cation radical that was further characterized by its accurate m/z 149.0616 from a high-resolution CID-MS^2 spectrum (Figure 1a). Similarly, electrospray of 9-iodomethyladenine from a D_2O/CD_3CN solution generated an H/D-exchanged 9-iodomethyladenine ion at m/z 279 that produced a $C_6H_4D_3N_5$ ion (m/z 152) upon CID (Figure 1b). To further enhance adenine protonation selectivity,[31,32] we also considered protonated complexes of 9-methyladenine with 2,3:11,12-dibenzo-18-crown-6-ether (DBCE) where hydrogen bonding to the crown ether greatly favors conformers of the N-1−H

https://dx.doi.org/10.1021/acs.jpca.0c10293
J. Phys. Chem. A 2021, 125, 338−348

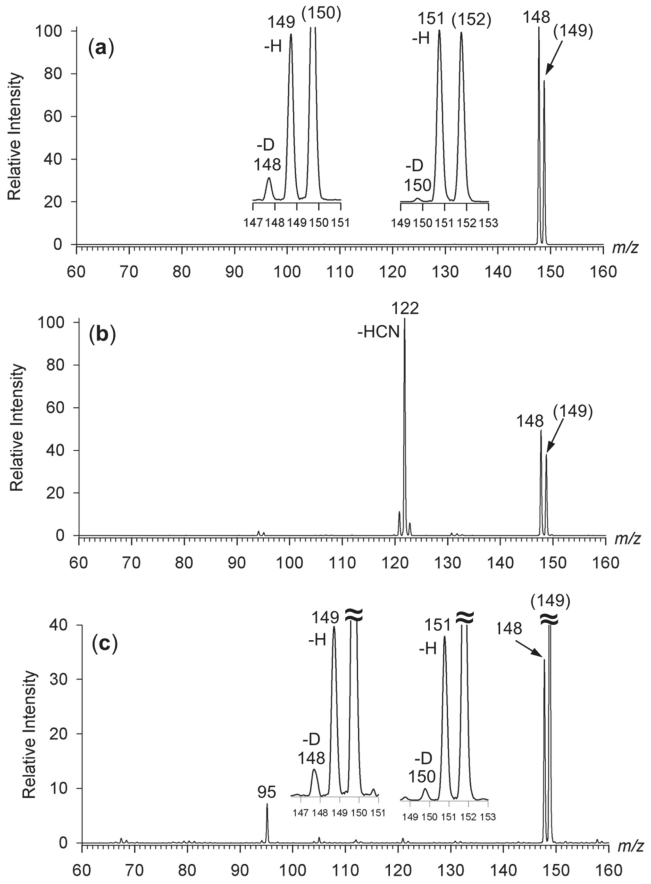

Figure 2. (a, b) CID-MS^3 spectra of (a) $C_6H_7N_5^{+\cdot}$ cation radical from 9-iodomethyladenine and (b) $[9\text{-methyladenine}]^{+\cdot}$ cation radical from the $[Cu(tpy)(9\text{-methyladenine})]^{2+\cdot}$ complex (ref 33). (c) UVPD-MS^3 (250 nm) spectrum of the $C_6H_7N_5^{+\cdot}$ cation radical from 9-iodomethyladenine. Insets in panels (a) and (c) show the loss of H/D from the [8-D] (m/z 150) and [N-D_3] (m/z 152) ions.

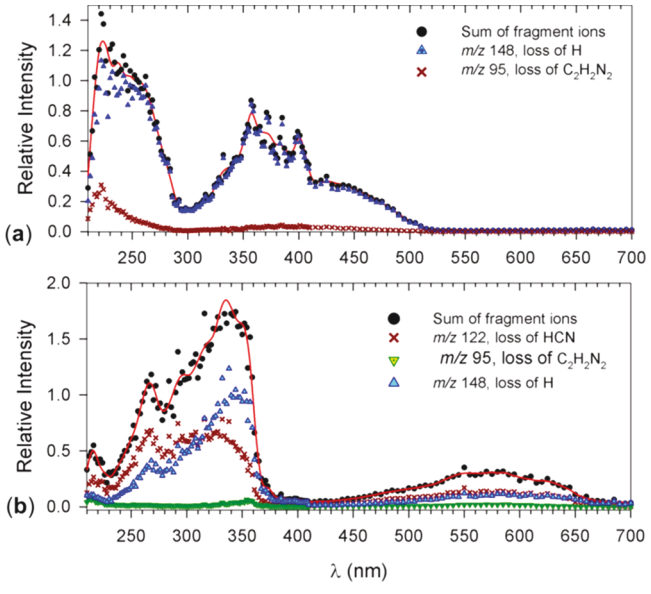

Figure 3. (a, b) UV−vis photodissociation action spectra of (a) $C_6H_7N_5^{+\cdot}$ from 9-iodomethyladenine and (b) canonical 9-methyladenine cation radical $\mathbf{1}^{+\cdot}$ (ref 33).

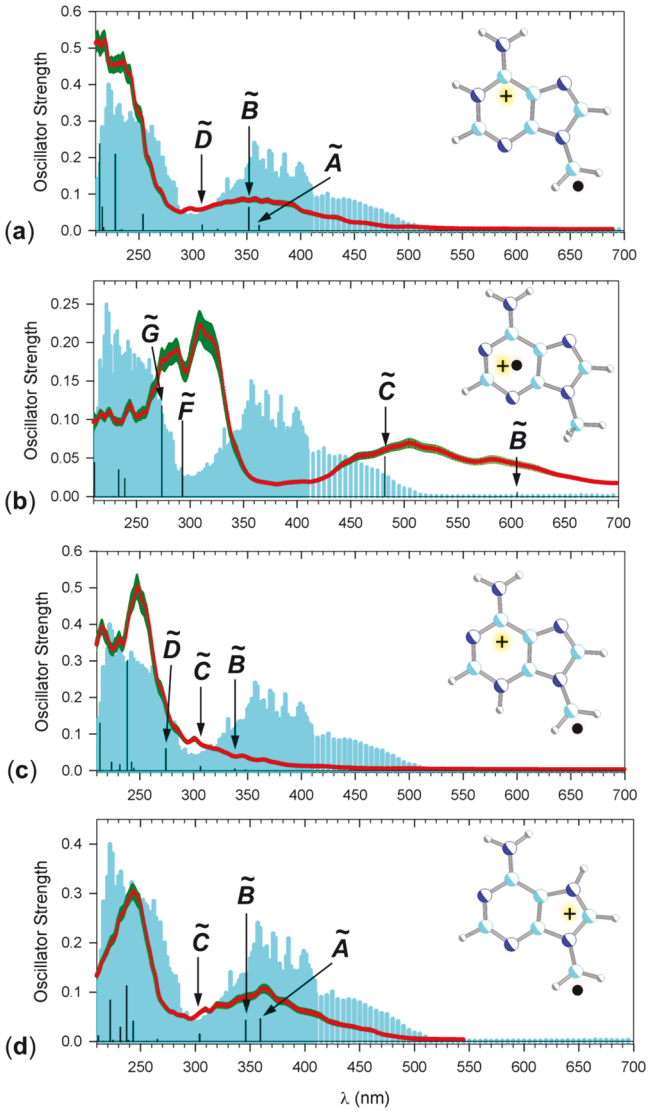

Figure 4. (a−d) M06-2X/6-31+G(d,p)-calculated vibronic spectra (310 K) of (a) $\mathbf{2}^{+\cdot}$, (b) $\mathbf{1}^{+\cdot}$, (c) $\mathbf{3}^{+\cdot}$, and (d) $\mathbf{4}^{+\cdot}$. The cyan background is an overlay of the action spectrum of $C_6H_7N_5^{+\cdot}$. The excited states were assigned from the comparison of M06-2X TD-DFT and EOM-CCSD calculations.

protomer (Tables S1 and S2 and Figures S1 and S2, Supporting Information). Electrospray ionization of 9-iodomethyladenine with DBCE produced the noncovalent complex ion (m/z 636) that was converted into $C_6H_7N_5^{+\cdot}$ in two consecutive CID steps, first eliminating DBCE and then iodine (Figure S3a,b, Supporting Information). Two steps with intermediate ion isolation were necessary to overcome the low-mass cutoff limit of the ion trap.

The $C_6H_7N_5^{+\cdot}$ ion was further characterized by its CID-MS^3 spectrum, which showed a single dissociation by loss of H (Figure 2a). Loss of H upon CID was also prevalent (>98%) from the N-D_3-exchanged ion at m/z 152 and abundant from the [8-D] ion (m/z 150), which showed a 12/88 ratio for D and H loss (Figure 2a, insets). The CID spectrum of the $C_6H_7N_5^{+\cdot}$ ion was clearly distinct from that of the canonical isomer, $[9\text{-methyladenine}]^{+\cdot}$ (Figure 2b).[33] The latter showed a prominent fragment ion by elimination of HCN (m/z 122) that was absent in the Figure 2a CID spectrum. Loss of H was also the main photodissociation (UVPD) of $C_6H_7N_5^{+\cdot}$ where it was

https://dx.doi.org/10.1021/acs.jpca.0c10293
J. Phys. Chem. A 2021, 125, 338−348

Table 1. Relative, Dissociation, and Transition-State Energies of Adenine Cation Radicals

	relative energy[a,b]			
species/reaction	M06-2X/6-311++G(2d,p)	CCSD(T)/[c]aug-cc-pVTZ	CCSD(T)/[c]aug-cc-pVQZ	CCSD(T)/[d]CBS
$\mathbf{1}^{+\cdot}$	6.0	5.3	6.7	6.4
$\mathbf{2}^{+\cdot}$	0	0	0	0
$\mathbf{3}^{+\cdot}$	10	10	9.8	9.9
$\mathbf{4}^{+\cdot}$	30	31	30	30
$\mathbf{2a}^{+}$ + H$^{\cdot}$	305	298	300	303
$\mathbf{2b}^{+}$ + H$^{\cdot}$	371	358	360	363
$\mathbf{2c}^{+}$ + H$^{\cdot}$	468	474	478	481
$\mathbf{2d}^{+}$ + H$^{\cdot}$	348	346	348	352
$\mathbf{5}^{+}$ + $H_2C{=}N{-}CN$	293	281	284	286
$\mathbf{2}^{+\cdot}$ → **TS1**	164	165	167	166
$\mathbf{2e}^{+\cdot}$	124	128	130	128
$\mathbf{2}^{+\cdot}$ → **TS2**	170	158	159	161
$\mathbf{2f}^{+\cdot}$	49	51	53	53
$\mathbf{2}^{+\cdot}$ → **TS3**	148	152	153	154
$\mathbf{2g}^{+\cdot}$	44	48	50	50
$\mathbf{2}^{+\cdot}$ → **TS4**	181	186	189	190
$\mathbf{2}^{+\cdot}$ → **TS5**	182	187	190	191
$\mathbf{2h}^{+}$ + H$^{\cdot}$	160	158	160	159

[a]In kJ mol^{-1}. [b]Including B3LYP zero-point energies scaled by 0.975 and referring to 0 K. [c]From extrapolation: E[CCSD(T)/aug-cc-pVXZ)] ≈ E[CCSD(T)/aug-cc-pVDZ)] + E[PMP2/aug-cc-pVXZ)] − E[PMP2/aug-cc-pVDZ)]. [d]Extrapolated to the complete basis set: E[CCSD(T)/CBS)] = E[CCSD(T)/aug-cc-pVDZ)] − E[PMP2/aug-cc-pVDZ)] + E[HF/aug-cc-pVQZ] + $E_{corr,X\to\infty}$.

Scheme 4. High-Energy Dissociations of $2^{+\cdot}$[a]

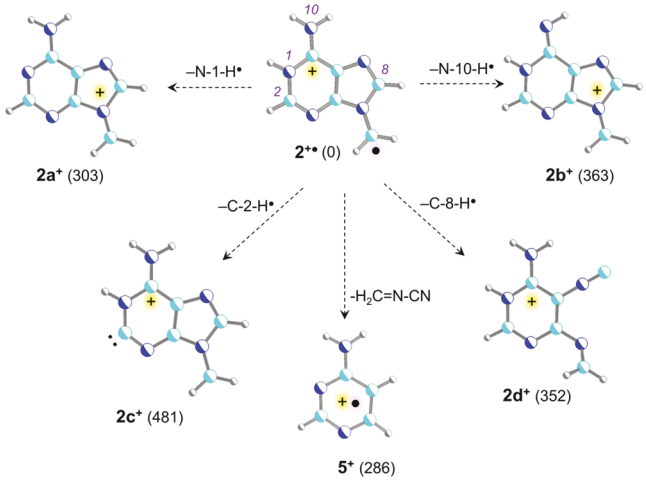

[a]M06-2X/6-31+G(d,p) optimized structures with relative energies in kJ mol^{-1} from CCSD(T)/CBS + ZPVE calculations.

accompanied by a minor elimination of $C_2H_2N_2$ (m/z 95, Figure 2c) from both the unlabeled and [N-D_3] forms (Figure S4a,b, Supporting Information). The loss of D from the labeled ions showed a slightly increased D/H ratios, 7/93 and 14/86 for the [N-D_3] and [8-D] ions, respectively (Figure 2c, insets) The overall MS^3 results strongly indicated that the $C_6H_7N_5^{+\cdot}$ ion was different from the canonical [9-methyladenine]$^{+\cdot}$ isomer.

Action Spectra. The m/z 148 and m/z 95 fragment ions identified in the CID and UVPD spectra were selected to monitor the action spectra of the $C_6H_7N_5^{+\cdot}$ ions in the 210−700 nm region. We obtained action spectra for $C_6H_7N_5^{+\cdot}$ ions generated from both 9-iodomethyladenine (Figure 1a) and its complex with DBCE (Figure S3b, Supporting Information). The spectra were identical, as documented by comparing the Figure 3a and Figure S5 data, indicating that the same ions were generated by both methods. The action spectrum of $C_6H_7N_5^{+\cdot}$ showed a composite band with maxima at 220 and 260 nm, several bands in the 340−410 nm region, and a shoulder at 440 nm extending to 510 nm. These bands were represented in both mass-resolved photodissociation channels, with the m/z 95 fragment ion contributing more to the 220 nm band (Figure 3a). The action spectrum of $C_6H_7N_5^{+\cdot}$ markedly differed from the previously reported spectrum of $\mathbf{1}^{+\cdot}$,[33] which showed prominent bands with maxima at 335 and 580 nm (Figure 3b). These bands were not represented in the action spectrum of $C_6H_7N_5^{+\cdot}$.

Ion Structures and Action Spectral Assignment. To assign structure to the new $C_6H_7N_5^{+\cdot}$ ion, we considered several isomers for which we calculated theoretical vibronic absorption spectra for excitations in thermal ions at 310 K (Figure 4). Transitions were assigned on the basis of comparing the TD-DFT and EOM-CCSD excited-state calculations (Figure S6, Supporting Information). The calculated spectra unambiguously distinguished $\mathbf{2}^{+\cdot}$ from $\mathbf{1}^{+\cdot}$ and $\mathbf{3}^{+\cdot}$. In particular, excitation to the A and B states of $\mathbf{2}^{+\cdot}$ at 361 and 352 nm, respectively (Figure 4a), accounted for the near-UV band in the action spectrum, while $\mathbf{1}^{+\cdot}$ and $\mathbf{3}^{+\cdot}$ did not have adequate transitions in this wavelength region. The intense transitions of $\mathbf{2}^{+\cdot}$ at 200, 213, 216, and 228 nm accounted for the dominant composite band at 210−250 nm in the action spectrum. Conversely, transitions to the F and G excited states of $\mathbf{1}^{+\cdot}$ (Figure 4b) and $\mathbf{3}^{+\cdot}$ (Figure 4c) were outside the absorption region of $\mathbf{2}^{+\cdot}$. Overall, the vibronic spectrum of $\mathbf{2}^{+\cdot}$ provided the best match with the action spectrum of $C_6H_7N_5^{+\cdot}$ across the entire wavelength range. However, the calculated vibronic spectrum of the higher-energy tautomer $\mathbf{4}^{+\cdot}$ also showed absorption bands matching the action spectrum, namely, for the 359 and 346 nm transitions to the A and B states, respectively (Figure 4d). The match for $\mathbf{4}^{+\cdot}$ was poorer for the strong experimental band at 220 nm. Based on its unique CID-MS^2 and action spectrum, the $C_6H_7N_5^{+\cdot}$ ion was identified as having a noncanonical structure of a distonic ion represented by the global energy minimum of an N-1-protonated adenine radical $\mathbf{2}^{+\cdot}$ or possibly the higher-energy isomer $\mathbf{4}^{+\cdot}$.

https://dx.doi.org/10.1021/acs.jpca.0c10293
J. Phys. Chem. A 2021, 125, 338−348

Scheme 5. Proposed Mechanism for H Loss Dissociation of $2^{+\bullet}$.[a]

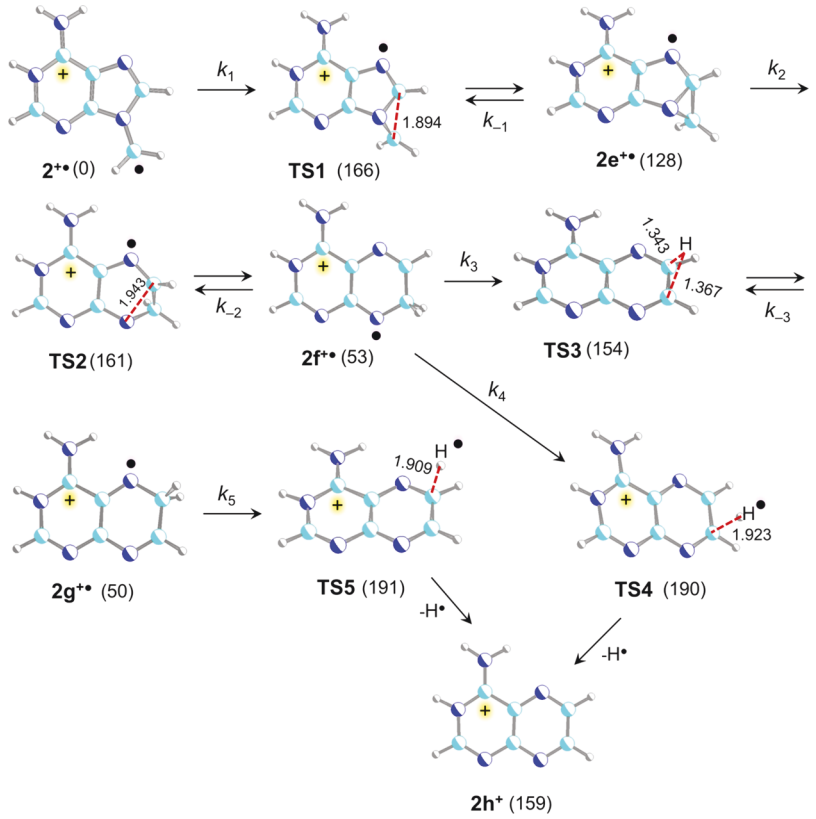

[a]M06-2X/6-31+G(d,p) optimized structures with relative energies in kJ mol^{-1} from CCSD(T)/CBS + ZPVE calculations.

The electronic transitions in $\mathbf{2}^{+\cdot}$ and $\mathbf{4}^{+\cdot}$ were investigated by molecular orbital (MO) analysis of the low excited states (Figure S7, Supporting Information). In both ions, the first (A) excited state resulted in dipole-allowed electron transitions from the singly occupied MO (SOMO39α) to the lowest unoccupied MO (LUMO40α) that were of the $\pi_z \rightarrow \pi_z^*$ type. Differences were apparent for the transitions within the β-orbital manifold, MO38$\beta \rightarrow$ MO39β, that corresponded to the D and B states at ΔE_{exc} = 4.02 and 3.58 eV for $\mathbf{2}^{+\cdot}$ and $\mathbf{4}^{+\cdot}$, respectively (Figure S7). In both $\mathbf{2}^{+\cdot}$ and $\mathbf{4}^{+\cdot}$, the SOMO had a large amplitude at the exocyclic CH_2 group, which was consistent with the high calculated atomic spin density at this carbon atom, 0.90 and 0.88 for $\mathbf{2}^{+\cdot}$ and $\mathbf{4}^{+\cdot}$, respectively. The electron transitions in $\mathbf{2}^{+\cdot}$ and $\mathbf{4}^{+\cdot}$ were fundamentally different from those in $\mathbf{1}^{+\cdot}$ (Figure S8, Supporting Information). The four lowest excited states in the canonical cation radical (A–D) involved internal electron transitions within the β-orbital manifold, out of which only the B (MO37$\beta \rightarrow$ MO39β) and C (MO36$\beta \rightarrow$ MO39β) states were of the $\pi_z \rightarrow \pi_z^*$ type to have oscillator strength allowing detection in the action spectrum. This feature further underscored the difference between $\mathbf{1}^{+\cdot}$ and its noncanonical isomers.

Ion Energies, Dissociation Mechanisms, and Product Ion Action Spectrum. We used ab initio calculations to establish the relative energies of cation radicals $\mathbf{1}^{+\cdot}$–$\mathbf{4}^{+\cdot}$ and to explore the parts of the potential energy surface that were relevant for the characteristic loss of hydrogen and competing dissociations. CCSD(T)/CBS relative energies are discussed in the text and schemes, and energies obtained at other levels of theory are compiled in Table 1. Ion $\mathbf{2}^{+\cdot}$ was the global energy minimum of the adenine-related $C_6H_7N_5^{+\cdot}$ ions, closely followed by $\mathbf{1}^{+\cdot}$ and $\mathbf{3}^{+\cdot}$. The N-7–H isomer $\mathbf{4}^{+\cdot}$ was 30 kJ mol^{-1} less stable than $\mathbf{2}^{+\cdot}$. Threshold and transition-state (TS) energies were obtained for the loss of H from different positions of $\mathbf{2}^{+\cdot}$, $\mathbf{3}^{+\cdot}$, and $\mathbf{4}^{+\cdot}$; those for $\mathbf{2}^{+\cdot}$ are discussed here.

Loss of H from N-1, NH_2, C-2, and C-8 was calculated to require high threshold energies, forming fragment ions $\mathbf{2a}^+$, $\mathbf{2b}^+$, $\mathbf{2c}^+$, and $\mathbf{2d}^+$, respectively (Scheme 4). This was consistent with the labeling data that showed lack of D loss from exchangeable (N-1–D and ND_2) positions. However, the very high threshold energy for the loss of C-2–H, leading to a triplet ion $\mathbf{2c}^+$, did not provide a plausible explanation for the ion dissociation. The calculated threshold energies for loss of H are to be compared with the threshold energy for the ring cleavage and elimination of $H_2C{=}N{-}CN$, forming ion $\mathbf{5}^+$ that corresponds to the very minor m/z 95 ion in the CID-MS^3 spectrum. These results suggested that a direct loss of H from $\mathbf{2}^{+\cdot}$ was energetically unfavorable, and the dissociation must follow a different mechanistic pathway to outcompete the ring cleavage while being consistent with the labeling data.

We propose an indirect mechanism (Scheme 5), which is compatible with the labeling data and reaction energetics and is supported by the reaction kinetics (*vide infra*). In the first step, the radical carrying a CH_2 group in $\mathbf{2}^{+\cdot}$ is assumed to cyclize to C-8, forming an aziridine ring in intermediate $\mathbf{2e}^{+\cdot}$ at 128 kJ mol^{-1} relative to $\mathbf{2}^{+\cdot}$. The cyclization proceeds through **TS1** at 166 kJ mol^{-1} relative to $\mathbf{2}^{+\cdot}$. The aziridine ring in $\mathbf{2e}^{+\cdot}$ is opened via **TS2** at 161 kJ mol^{-1} relative to $\mathbf{2}^{+\cdot}$ (33 kJ mol^{-1} relative to $\mathbf{2e}^{+\cdot}$), resulting in a ring expansion and forming the dihydropteridine intermediate $\mathbf{2f}^{+\cdot}$ at 53 kJ mol^{-1}. Ion $\mathbf{2f}^{+\cdot}$ can undergo facile reversible isomerization by 1,2-H atom shift between the CH_2 group and C-8, proceeding via **TS3** at 154 kJ mol^{-1} and forming

https://dx.doi.org/10.1021/acs.jpca.0c10293
J. Phys. Chem. A 2021, 125, 338–348

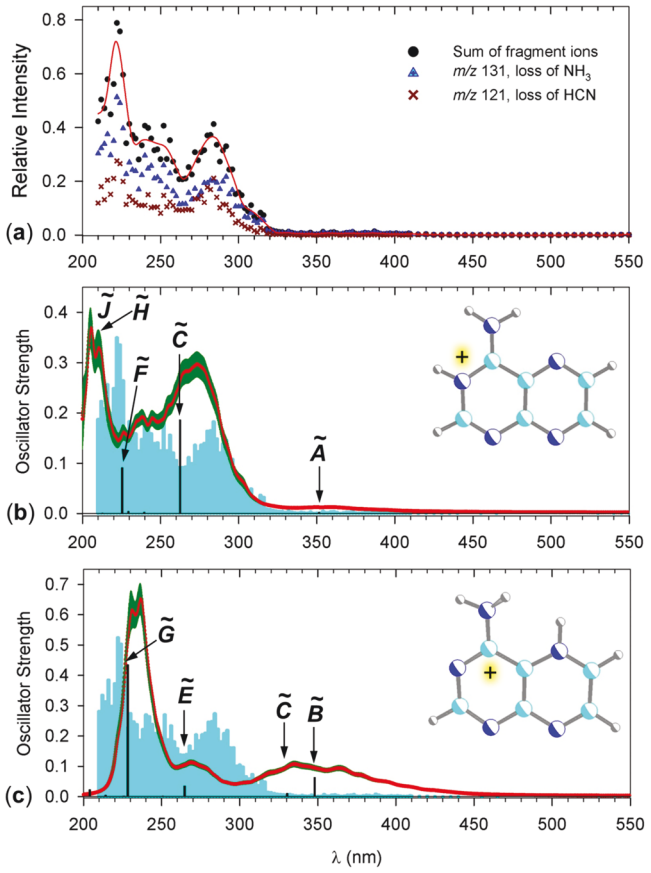

Figure 5. (a) UV−vis action spectrum of m/z 148 ($C_6H_6N_5^+$) ion by loss of H from $\mathbf{2}^{+\cdot}$. (b, c) M06-2X/6-31+G(d,p)-calculated vibronic spectra (310 K) of (b) $\mathbf{2h}^+$ and (c) $\mathbf{4d}^+$. The cyan background is an overlay of the action spectrum of $C_6H_6N_5^+$.

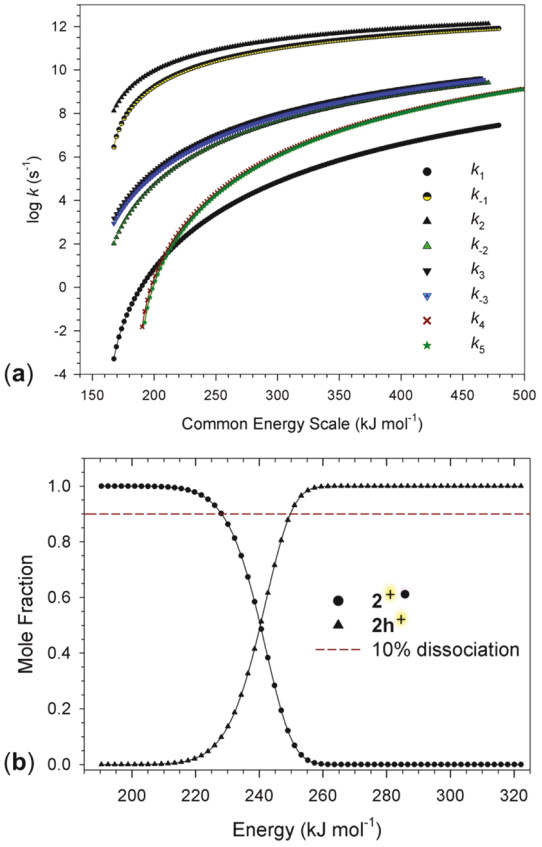

Figure 6. (a) RRKM rate constants pertinent to Scheme 5 reactions plotted on a common energy scale relative to $\mathbf{2}^{+\cdot}$. (b) Calculated mole fractions of the $\mathbf{2}^{+\cdot}$ reactant and $\mathbf{2h}^+$ product after 50 ms in the ion trap.

dihydropteridine ion $\mathbf{2g}^{+\cdot}$ at 50 kJ mol^{-1} relative to $\mathbf{2}^{+\cdot}$. Finally, loss of H from the ring CH_2 groups in $\mathbf{2f}^{+\cdot}$ and $\mathbf{2g}^{+\cdot}$ required 190 and 191 kJ mol^{-1} in **TS4** and **TS5**, respectively, to form a common product, which is an N-1-protonated aminopteridine $\mathbf{2h}^+$ at 159 kJ mol^{-1} relative to $\mathbf{2}^{+\cdot}$. Note that we retain the adenine ring atom numbering for the aminopteridine dissociation products. The salient feature of the Scheme 5 mechanism was that all the TS and threshold energies were substantially lower than the threshold energy for the ring cleavage leading to elimination of $H_2C{=}N{-}CN$ (Table 1). Thus, the Scheme 5 mechanism was consistent with the CID-MS^3 spectrum. We also considered alternative mechanisms of H atom loss, but those required high TS energies (**TS6**−**TS9**), as described in detail in the Supporting Information (Schemes S3 and S4). Loss of H from the N-7-H protomer $\mathbf{4}^{+\cdot}$ was also evaluated by its energetics and kinetics as visualized in Scheme S5 and Figures S9 and S10 (**TS10**−**TS14**, Supporting Information).

Experimental evidence for the proposed mechanism was sought by determining the structure of the m/z 148 product ion by CID-UVPD-MS^4 action spectroscopy. The action spectrum showed two major photodissociation channels leading to loss of NH_3 (m/z 131) and HCN (m/z 121), forming bands with maxima at 285, 250, and 220 nm (Figure 5a). The spectrum of this ion was different from that obtained for the m/z 148 ion generated by CID-MS^3 from [9-methyladenine]$^{+\cdot}$ (Figure S11, Supporting Information). Significantly, the absorption bands in the action spectrum were matched by the calculated bands in the vibronic spectrum of $\mathbf{2h}^+$ (Figure 5b). The latter showed a weak transition to the A state at 351 nm and more intense transitions to the C, F, and H states at 262, 225, and 196 nm, respectively. Upon vibronic redshift and broadening, these transitions gave rise to bands matching the prominent features in the action spectrum. In contrast, the spectrum of the N-7-protonated pteridine ion $\mathbf{4d}^+$ showed a major mismatch with the action spectrum. For example, the intense transitions to the B and G states at 348 and 228 nm, respectively (Figure 5c), did not match the bands in the action spectrum. In particular, the absence in the action spectrum of the 348 nm band excluded the N-7-protonated isomers for the m/z 148 and, by implication, also its precursor $\mathbf{4}^{+\cdot}$. Hence, UV−vis action spectroscopy alone proved to be sufficient for resolving the protomeric forms and allowed us to assign structure $\mathbf{2}^{+\cdot}$ to the noncanonical adenine cation radical. It is fair to note that structures $\mathbf{2}^{+\cdot}$ and $\mathbf{4}^{+\cdot}$ are theoretically distinguishable by infrared spectra that show different bands for the N-1−H and N-7−H stretching and in-plane bending modes in the calculated spectra (Figure S12, Supporting Information). Structures $\mathbf{2}^{+\cdot}$ and $\mathbf{4}^{+\cdot}$ thus present a future challenge to be addressed by infrared action spectroscopies.

Dissociation Kinetics. To quantitatively evaluate the Scheme 5 mechanism, we utilized the CCSD(T)/CBS-calculated potential energy surface for the H atom loss from $\mathbf{2}^{+\cdot}$ to calculate unimolecular rate constants, by the Rice−Ramsperger−Kassel−Marcus theory model.[56] The rate constants (log k) for the reversible reactions, $\mathbf{2}^{+\cdot} \leftrightarrow$ **TS1** $\leftrightarrow \mathbf{2e}^{+\cdot}$ (k_1, k_{-1}), $\mathbf{2e}^{+\cdot} \leftrightarrow$ **TS2** $\leftrightarrow \mathbf{2f}^{+\cdot}$ (k_2, k_{-2}), and $\mathbf{2f}^{+\cdot} \leftrightarrow$ **TS3** $\leftrightarrow \mathbf{2g}^{+\cdot}$ (k_3, k_{-3}), and the exit channels, $\mathbf{2f}^{+\cdot} \rightarrow$ **TS4** $\rightarrow \mathbf{2h}^+ + H^\cdot$ (k_4) and $\mathbf{2g}^{+\cdot} \rightarrow$ **TS5** $\rightarrow \mathbf{2h}^+ + H^\cdot$ (k_5), (Scheme 5) were plotted on a

https://dx.doi.org/10.1021/acs.jpca.0c10293
J. Phys. Chem. A 2021, 125, 338−348

Scheme 6. Kinetic Analysis of the Distribution of D-Labeled Intermediates and Rate Constants for Competitive Loss of H and D

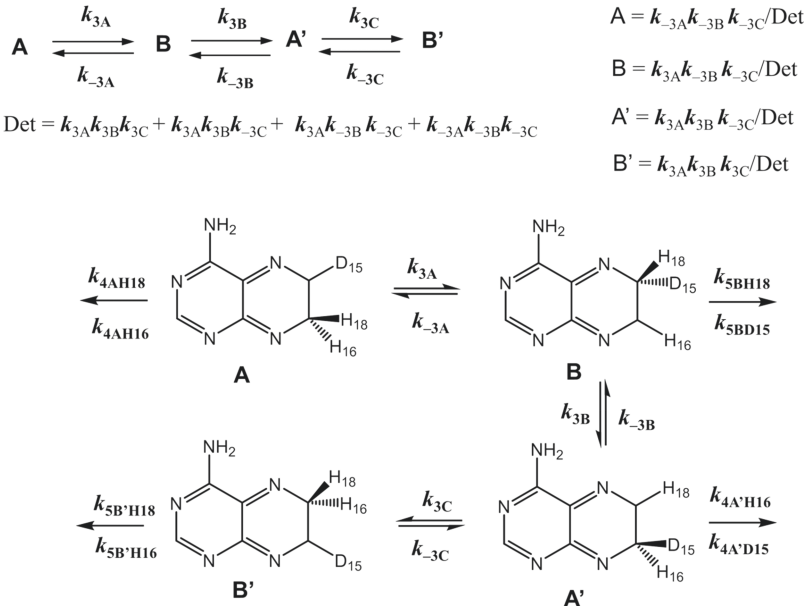

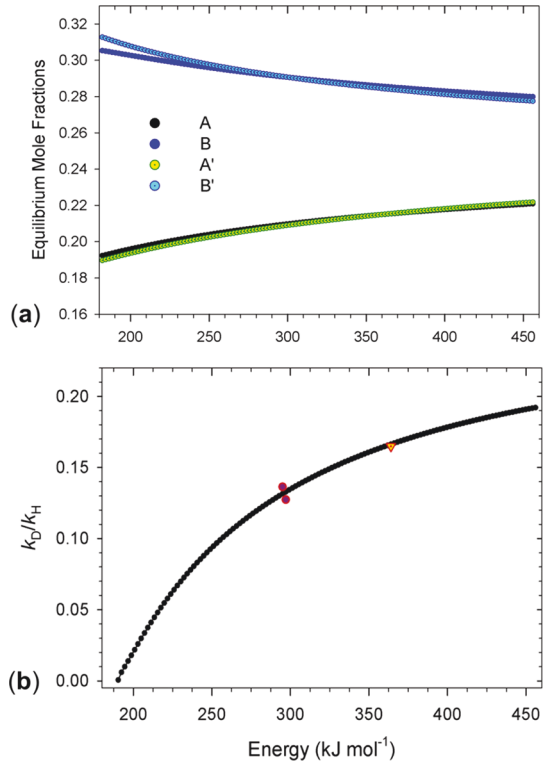

Figure 7. (a) Equilibrium populations of $\mathbf{2f}^{+\cdot}$ and $\mathbf{2g}^{+\cdot}$ isotopologues **A**, **A′**, **B**, and **B′**. (b) Calculated ratio of rate constants for loss of H (k_H) and D (k_D) from an equilibrium mixture of $\mathbf{2f}^{+\cdot}$ and $\mathbf{2g}^{+\cdot}$ isotopologues **A**, **A′**, **B**, and **B′** according to Scheme 6. The experimental data are shown as circles (CID) and upside triangle (UVPD at 270 nm).

common energy scale and are shown in Figure 6a. The rate constants indicated that the rate-determining steps for the dissociation were the ring closure in $\mathbf{2}^{+\cdot}$ (k_1) and the C−H bond cleavages in $\mathbf{2f}^{+\cdot}$ (k_4) and $\mathbf{2g}^{+\cdot}$ (k_5), while the reversible interconversion of $\mathbf{2f}^{+\cdot}$ and $\mathbf{2g}^{+\cdot}$ (k_3, k_{-3}) was >2 orders of magnitude faster at all relevant internal energies of $\mathbf{2}^{+\cdot}$. Under these conditions, the populations of $\mathbf{2}^{+\cdot}$, $\mathbf{2f}^{+\cdot}$, and $\mathbf{2g}^{+\cdot}$ preceding

Table 2. Relative Free Energies, Absolute Adiabatic Recombination Energies, and M06-2X Optimized Structures of Adenosine Cation Radicals[e]

	relative energy[a,b]	
ion	M06-2X/6-311++G(2d,p)	CCSD(T)/CBS
$\mathbf{Ad1}^{+\cdot}$	0 (0)[c], (7.76)[d], (6.26)[c,d]	0 (7.82)[d]
$\mathbf{Ad2}^{+\cdot}$	−29 (−42)[c], (4.12)[d], (3.17)[c,d]	−23 (4.42)[d]
$\mathbf{Ad3}^{+\cdot}$	−38 (−35)[c], (4.65)[d], (3.46)[c,d]	−39 (4.74)[d]
$\mathbf{Ad4}^{+\cdot}$	−27 (−33)[c], (4.88)[d], (3.29)[c,d]	−19 (5.10)[d]

[a]In kJ mol^{-1} unless stated otherwise. [b]Including zero-point energies, enthalpies, and entropies at 310 K. [c]Including solvation energies in water. [d]Absolute adiabatic recombination energies in eV. [e]

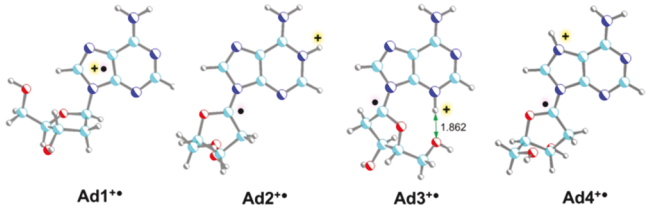

dissociation can be considered to be close to a dynamic equilibrium to simplify the dissociation kinetics, where the energy-dependent mole fractions of $\mathbf{2f}^{+\cdot}$ and $\mathbf{2g}^{+\cdot}$ are functions of k_1, k_{-1}, k_2, k_{-2}, k_3, and k_{-3}. When combined with the rate constants for the rate-determining steps of H atom loss, k_4 and k_5, respectively, we can calculate the energy-dependent mole fractions of the reactant ($\mathbf{2}^{+\cdot}$) and products ($\mathbf{2h}^{+}$ + H$^{\cdot}$) after 50 ms of the ion residence time in the ion trap (Figure 6b). The Figure 6b data indicated that >10% dissociation was achieved in ions having >230 kJ mol^{-1} internal energy and the dissociation was complete in ions having 260 kJ mol^{-1}. These figures were reasonable considering the typical collisional excitation in 3D ion traps.[65−67] The calculated range of the kinetically limited ion internal energies was also consistent with photoexcitation, allowing single-photon dissociation at laser wavelengths up to 520 nm. This was fully compatible with the UV−vis action spectrum (Figure 3a).

https://dx.doi.org/10.1021/acs.jpca.0c10293
J. Phys. Chem. A 2021, 125, 338−348

Isotope Effects. We further used the equilibrium formation of $\mathbf{2f}^{+\cdot}$ and $\mathbf{2g}^{+\cdot}$ to address the isotope effects on the competitive loss of H and D from [8-D]-$\mathbf{2}^{+\cdot}$ (Figure 2a). Equilibrium populations were calculated for intermediates **A**, **B**, **A′**, and **B′** (Scheme 6), in which the D atom (D15), originally placed at C-8, was distributed by reversible H and D migrations with rate constants k_{3A}, k_{-3A}, k_{3B}, k_{-3B}, k_{3C}, and k_{-3C}, (Figure 7a) followed by dissociation with rate constants $k_{4AH18} = k_{4AH16}$, k_{5BH18}, $k_{4A'H16}$, and $k_{5B'H18} = k_{5B'H16}$ for loss of H. The loss of D was analogously expressed by rate constants k_{5BD15} and $k_{4A'D15}$. All these rate constants were calculated including primary and secondary isotope effects with appropriate zero-point energies, vibrational frequencies, and moments of inertia of the D-containing intermediates and the pertinent transition states (**TS3**, **TS4**, and **TS5**). The results are summarized as the energy-dependent k_D/k_H ratio, expressing the overall loss of D and H (Figure 7b). This showed that the fraction of D loss increased with ion internal energy, which was caused by a combination of kinetic factors, such as the increasing population of intermediate **A′** that can dissociate by D loss and the lower kinetic isotope effect affecting this dissociation. The experimental ratio for collisional activation ($k_D/k_H = 12/88 = 0.136$) was matched at the internal energy of 295 kJ mol^{-1}. The ratio for photoexcitation (14/86 = 0.163) was matched at 360 kJ mol^{-1}. This was less than the photon energy used to obtain the photodissociation spectrum (443 kJ mol^{-1}), but the difference can be accounted for by ion collisional cooling after photon absorption during the 50 ms ion storage time.[67,68]

Distonic Isomers of 2′-Deoxyadenosine Cation Radicals. The specific generation and stability of the elusive distonic isomer of 9-methyladenine cation radical, along with those of thymine[14] and methylcytosine,[15] indicated that nontraditional structures may play a role in DNA oxidation. To investigate this unusual aspect of nucleobase cation radical chemistry, we investigated the structures and relative energies of 2′-deoxyadenosine isomers produced by H atom migrations in the canonical structure $\mathbf{Ad1}^{+\cdot}$. The lowest-energy 2′-deoxyribose conformers for each nucleobase tautomer were selected after Born−Oppenheimer molecular dynamics trajectory calculations and optimized by DFT calculations. Here, we report CCSD(T)/CBS energies with zero-point corrections, enthalpies, and entropies at 310 K. The calculated free energies (Table 2) indicated a substantial stabilization of the noncanonical isomers $\mathbf{Ad2}^{+\cdot}$ and $\mathbf{Ad3}^{+\cdot}$ relative to $\mathbf{Ad1}^{+\cdot}$ in both the gas phase and solvation by water. Structures $\mathbf{Ad2}^{+\cdot}$−$\mathbf{Ad4}^{+\cdot}$ have the protonation (N-1, N-3, or N-7) and radical (C-1′) sites on separate atoms and thus represent stable distonic ions.[69,70] Their enhanced stability relative to that of $\mathbf{Ad1}^{+\cdot}$ can be related to the difference in the N−H and C-1′−H bond dissociation energies in protonated adenosines. The available energy data placed the 298 K dissociation energy of the C-1′−H bond in 2′-deoxyribofuranose at 384 kJ mol^{-1}.[71] This is to be compared with the 298 K energies for homolytic dissociation of the N-1−H, N-3−H, and N-7−H bonds in protonated 9-methyladenines that we calculated with CCSD(T)/CBS as 420, 412, and 395 kJ mol^{-1}, respectively. These energies indicated that a hydrogen atom transfer from C-1′ to the adenine nitrogen positions was also exothermic in ionized $\mathbf{Ad1}^{+\cdot}$, leading to the noncanonical structures $\mathbf{Ad2}^{+\cdot}$−$\mathbf{Ad4}^{+\cdot}$. The Table 2 data for 2′-deoxyadenosine further revealed that the stability of $\mathbf{Ad2}^{+\cdot}$−$\mathbf{Ad4}^{+\cdot}$ relative to $\mathbf{Ad1}^{+\cdot}$ was retained after including solvation with water. Thus, the findings for gas-phase 9-methyladenine cation radicals can be extended to the case of nucleoside ions. The potential importance of the noncanonical nucleoside cation radical isomers stems from their recombination energies that affect electron transfer in ionized DNA. For the canonical isomer $\mathbf{Ad1}^{+\cdot}$, we calculated an adiabatic recombination energy (RE_a, given as an absolute value) of 7.82 eV, which was between those of guanosine (7.49−7.51 eV),[72] thymidine (8.12 eV), and cytidine (8.14 eV). Thus, $\mathbf{Ad1}^{+\cdot}$ can abstract an electron from guanosine and promote the ionization site moving along the DNA molecule. In contrast, the low-energy isomers $\mathbf{Ad2}^{+\cdot}$ and $\mathbf{Ad3}^{+\cdot}$ have very low RE_a, 4.41 and 4.73 eV, respectively. If formed in ionized DNA, these cation radicals would function as hole traps that would not engage in electron transfer along the backbone or in the Watson−Crick pairs.

CONCLUSIONS

In conclusion, noncanonical isomers of 9-methyladenine and adenosine cation radicals represent new low-energy species of distinct electronic properties. The noncanonical 9-methylene-(1*H*)adenine cation radical was generated for the first time using targeted gas-phase ion chemistry, and its structure was entirely characterized by UV−vis photodissociation action spectroscopy. The discovery of stable noncanonical nucleobase and nucleoside cation radicals presents a challenge for future experimental and computational studies to search for the formation and role of such noncanonical intermediates in DNA ionization.

ASSOCIATED CONTENT

Supporting Information

The Supporting Information is available free of charge at https://pubs.acs.org/doi/10.1021/acs.jpca.0c10293.

Description of synthetic procedures, compound characterization, auxiliary figures of mass spectra, excited-state calculations, table of energies, RRKM calculations and discussion of kinetics, molecular orbitals, and UV−vis action and IR spectra (PDF)

AUTHOR INFORMATION

Corresponding Authors

Aleš Marek − *Institute of Organic Chemistry and Biochemistry, The Czech Academy of Sciences, 16610 Prague 6, Czech Republic*; Email: ales.marek@uochb.cas.cz

František Tureček − *Department of Chemistry, University of Washington, Seattle, Washington 98195-1700, United States*; orcid.org/0000-0001-7321-7858; Phone: +1-206-685-2041; Email: turecek@uw.edu

Authors

Shu R. Huang − *Department of Chemistry, University of Washington, Seattle, Washington 98195-1700, United States*

Gabriela Nováková − *Institute of Organic Chemistry and Biochemistry, The Czech Academy of Sciences, 16610 Prague 6, Czech Republic*

Complete contact information is available at: https://pubs.acs.org/10.1021/acs.jpca.0c10293

Notes

The authors declare no competing financial interest.

ACKNOWLEDGMENTS

Research at the University of Washington was supported by the Chemistry Division of the U.S. National Science Foundation,

grants CHE-1951518 for experimental work and CHE-1661815 for computations. F.T. acknowledges support by the Klaus and Mary Ann Saegebarth Endowment. Research at the IOCB was supported by the Ministry of Education, Youth and Sport (MŠMT, Grant INTER-EXCELLENCE LTAUSA19094).

REFERENCES

(1) Yu, C.; O'Donnell, T. J.; LeBreton, P. R. Ultraviolet Photoelectron Studies of Volatile Nucleoside Models. Vertical Ionization Potential Measurements of Methylated Uridine, Thymidine, Cytidine, and Adenosine. *J. Phys. Chem.* **1981**, *85*, 3851−3855.

(2) Improta, R.; Scalmani, G.; Barone, V. Radical Cations of DNA Bases: Some Insights on Structure and Fragmentation Patterns by Density Functional Methods. *Int. J. Mass Spectrom.* **2000**, *201*, 321−336.

(3) Crespo-Hernández, C. E.; Arce, R.; Ishikawa, Y.; Gorb, L.; Leszczynski, J.; Close, D. M. Ab Initio Ionization Energy Thresholds of DNA and RNA Bases in Gas Phase and in Aqueous Solution. *J. Phys. Chem. A* **2004**, *108*, 6373−6377.

(4) Blancafort, L.; Voityuk, A. A. CASSCF/CAS-PT2 Study of Hole Transfer in Stacked DNA Nucleobases. *J. Phys. Chem. A* **2006**, *110*, 6426−6432.

(5) Slavíček, P.; Winter, B.; Faubel, M.; Bradforth, S. E.; Jungwirth, P. Ionization Energies of Aqueous Nucleic Acids: Photoelectron Spectroscopy of Pyrimidine Nucleosides and ab Initio Calculations. *J. Am. Chem. Soc.* **2009**, *131*, 6460−6467.

(6) Faber, C.; Attaccalite, C.; Olevano, V.; Runge, E.; Blase, X. First-PrinciplesGWCalculations for DNA and RNA Nucleobases. *Phys. Rev. B* **2011**, *83*, 115123−115123.

(7) Pluhařová, E.; Jungwirth, P.; Bradforth, S. E.; Slavíček, P. Ionization of Purine Tautomers in Nucleobases, Nucleosides, and Nucleotides: From the Gas Phase to the Aqueous Environment. *J. Phys. Chem. B* **2011**, *115*, 1294−1305.

(8) Tehrani, Z. A.; Javan, M. J.; Fattahi, A.; Hashemi, M. M. Effect of Cation Radical Formation on Reactivity and Acidity Enhancement of Cytosine Nucleobase: Natural Bond Orbital and Atom in Molecule Analysis. *J. Theor. Comput. Chem.* **2012**, *11*, 313−327.

(9) Pluhařová, E.; Schroeder, C.; Seidel, R.; Bradforth, S. E.; Winter, B.; Faubel, M.; Slavíček, P.; Jungwirth, P. Unexpectedly Small Effect of the DNA Environment on Vertical Ionization Energies of Aqueous Nucleobases. *J. Phys. Chem. Lett.* **2013**, *4*, 3766−3769.

(10) Cadet, J.; Wagner, J. R.; Shafirovich, V.; Geacintov, N. E. One-Electron Oxidation Reactions of Purine and Pyrimidine Bases in Cellular DNA. *Int. J. Rad. Biol.* **2014**, *90*, 423−432.

(11) Dawley, M. M.; Tanzer, K.; Cantrell, W. A.; Plattner, P.; Brinkmann, N. R.; Scheier, P.; Denifl, S.; Ptasińska, S. Electron Ionization of the Nucleobases Adenine and Hypoxanthine near the Threshold: A Combined Experimental and Theoretical Study. *Phys. Chem. Chem. Phys.* **2014**, *16*, 25039−25053.

(12) Schroeder, C. A.; Pluhařová, E.; Seidel, R.; Schroeder, W. P.; Faubel, M.; Slavíček, P.; Winter, B.; Jungwirth, P.; Bradforth, S. E. Oxidation Half-Reaction of Aqueous Nucleosides and Nucleotides via Photoelectron Spectroscopy Augmented by Ab initio Calculations. *J. Am. Chem. Soc.* **2015**, *137*, 201−209.

(13) Wang, Y.; Zhao, H.; Yang, C.; Jie, J.; Dai, X.; Zhou, Q.; Liu, K.; Song, D.; Su, H. Degradation of Cytosine Radical Cations in 2′-Deoxycytidine and in i-Motif DNA: Hydrogen-Bonding Guided Pathways. *J. Am. Chem. Soc.* **2019**, *141*, 1970−1979.

(14) Dang, A.; Nguyen, H. T. H.; Ruiz, H.; Piacentino, E.; Ryzhov, V.; Tureček, F. Experimental Evidence for Non-Canonical Thymine Cation Radicals in the Gas Phase. *J. Phys. Chem. B* **2018**, *122*, 86−97.

(15) Huang, S. R.; Tureček, F. Cation Radicals of Hachimoji Nucleobases. Canonical Purine and Non-Canonical Pyrimidine Forms Generated in the Gas Phase and Characterized by UV-Vis Photodissociation Action Spectroscopy. *J. Phys. Chem. A* **2020**, *124*, 7101−7112.

(16) Kim, N.-J. DFT Study of Water-Assisted Intramolecular Proton Transfer in the Tautomers of Thymine Radical Cation. *Bull. Korean Chem. Soc.* **2006**, *27*, 1009−1014.

(17) Lam, A. K. Y.; Abrahams, B. F.; Grannas, M. J.; McFadyen, W. D.; O'Hair, R. A. J. Tuning the Gas Phase Redox Properties of Copper(II) Ternary Complexes of Terpyridines to Control the Formation of Nucleobase Radical Cations. *Dalton Trans.* **2006**, 5051−5061.

(18) Feketeová, L.; Khairallah, G. N.; Chan, B.; Steinmetz, V.; Maître, P.; Radom, L.; O'Hair, R. A. J. Gas-Phase Infrared Spectrum and Acidity of the Radical Cation of 9-Methylguanine. *Chem. Commun.* **2013**, *49*, 7343−7345.

(19) Antoine, R.; Dugourd, P. UV-Visible Activation of Biomolecular Ions. *Lect. Notes Chem.* **2013**, *83*, 93−116.

(20) Antoine, R.; Dugourd, P. In *Photophysics of Ionic Biochromophores*; Nielsen, S. B.; Wyer, J. A. Eds.; Springer: Heidelberg, 2013, pp. 141−145.

(21) Shaffer, C. J.; Pepin, R.; Tureček, F. Combining UV Photodissociation Action Spectroscopy with Electron Transfer Dissociation for Structure Analysis of Gas-Phase Peptide Cation-Radicals. *J. Mass Spectrom.* **2015**, *50*, 1438−1442.

(22) Dunbar, R. C. Photodissociation of Trapped Ions. *Int. J. Mass Spectrom.* **2000**, *200*, 571−589.

(23) Baer, T.; Dunbar, R. C. Ion Spectroscopy: Where Did It Come From; Where Is It Now; and Where Is It Going? *J. Am. Soc. Mass Spectrom.* **2010**, *21*, 681−693.

(24) Rizzo, T. R.; Stearns, J. A.; Boyarkin, O. V. Spectroscopic Studies of Cold, Gas-Phase Biomolecular Ions. *Int. Rev. Phys. Chem.* **2009**, *28*, 481−515.

(25) Polfer, N.; Sartakov, B. G.; Oomens, J. The Infrared Spectrum of the Adamantyl Cation. *Chem. Phys. Lett.* **2004**, *400*, 201−205.

(26) Nizkorodov, S. A.; Dopfer, O.; Ruchti, T.; Meuwly, M.; Maier, J. P.; Bieske, E. J. Size Effects in Cluster Infrared Spectra: the ν_1 Band of Ar_n-HCO^+ (n = 1-13). *J. Phys. Chem.* **1995**, *99*, 17118−17129.

(27) DeBlase, A. F.; Bloom, S.; Lectka, T.; Jordan, K. D.; McCoy, A. B.; Johnson, M. A. Origin of the Diffuse Vibrational Signature of a Cyclic Intramolecular Proton Bond: Anharmonic Analysis of Protonated 1,8-Disubstituted Naphthalene Ions. *J. Chem. Phys.* **2013**, *139*, No. 024301.

(28) Nguyen, H. T. H.; Shaffer, C. J.; Pepin, R.; Tureček, F. UV Action Spectroscopy of Gas-Phase Peptide Radicals. *J. Phys. Chem. Lett.* **2015**, *6*, 4722−4727.

(29) Viglino, E.; Shaffer, C. J.; Tureček, F. UV/Vis Action Spectroscopy and Structures of Tyrosine Peptide Cation Radicals in the Gas Phase. *Angew. Chem., Int. Ed.* **2016**, *55*, 7469−7473.

(30) Huang, S. R.; Liu, Y.; Tureček, F. UV-Vis Photodissociation Action Spectroscopy Reveals Cytosine-Guanine Hydrogen Transfer in DNA Tetranucleotide Cation Radicals upon One-Electron Reduction. *J. Phys Chem. B* **2020**, *124*, 3505−3517.

(31) Korn, J. A.; Urban, J.; Dang, A.; Nguyen, H. T. H.; Tureček, F. UV/Vis Action Spectroscopy Reveals a Conformational Collapse in Hydrogen-Rich Dinucleotide Cation Radicals. *J. Phys. Chem. Lett.* **2017**, *8*, 4100−4107.

(32) Liu, Y.; Huang, S. R.; Tureček, F. Guanine-Adenine Interactions in DNA Tetranucleotide Cation Radicals Revealed by UV/Vis Photodissociation Action Spectroscopy and Theory. *Phys. Chem. Chem. Phys.* **2020**, *22*, 16831−16842.

(33) Huang, S. R.; Dang, A.; Tureček, F. Ground and Excited States of Gas-Phase DNA Nucleobase Cation-Radicals. A UV-Vis Photodisociation Action Spectroscopy and Computational Study of Adenine and 9-Methyladenine. *J. Am. Soc. Mass Spectrom.* **2020**, *31*, 1271−1281.

(34) Chyall, L. J.; Kenttämaa, H. I. Gas-Phase Reactions of the 4-Dehydroanilinium Ion and Its Isomers. *J. Mass Spectrom.* **1995**, *30*, 81−87.

(35) Petzold, C. J.; Nelson, E. D.; Lardin, H. A.; Kenttämaa, H. I. Charge-Site Effects on the Radical Reactivity of Distonic Ions. *J. Phys. Chem. A* **2002**, *106*, 9767−9775.

(36) Widjaja, F.; Jin, Z.; Nash, J. J.; Kenttämaa, H. I. Comparison of the Reactivity of the Three Distonic Isomers of the Pyridine Radical

Cation Toward Tetrahydrofuran in Solution and in the Gas Phase. *J. Am. Soc. Mass Spectrom.* **2013**, *24*, 469−480.
(37) Kotha, R. R.; Yerabolu, R.; Aqueel, M. S.; Riedeman, J. S.; Szalwinski, L.; Ding, D.; Nash, J. J.; Kenttämaa, H. I. Quinoline Triradicals: A Reactivity Study. *J. Am. Chem. Soc.* **2019**, *141*, 6672−6679.
(38) Dang, A.; Korn, J. A.; Gladden, J.; Mozzone, B.; Tureček, F. UV-Vis Photodissociation Action Spectroscopy on Thermo LTQ-XL ETD and Bruker amaZon Ion Trap Mass Spectrometers: A Practical Guide. *J. Am. Soc. Mass Spectrom.* **2019**, *30*, 1558−1564.
(39) Frisch, M. J.; Trucks, G. W.; Schlegel, H. B.; Scuseria, G. E.; Robb, M. A.; Cheeseman, J. R.; Scalmani, G.; Barone, V.; Petersson, G. A.; Nakatsuji, H.; et al. *Gaussian 16*, Revision A03; Gaussian, Inc.: Wallingford, CT, 2016.
(40) Becke, A. D. A New Mixing of Hartree-Fock and Local Density-Functional Theories. *J. Chem. Phys.* **1993**, *98*, 1372−1377.
(41) Yanai, T.; Tew, D. P.; Handy, N. C. A New Hybrid Exchange-Correlation Functional Using the Coulomb-Attenuating Method (CAM-B3LYP). *Chem. Phys. Lett.* **2004**, *393*, 51−57.
(42) Zhao, Y.; Truhlar, D. G. The M06 Suite of Density Functionals for Main Group Thermochemistry, Thermochemical Kinetics, Noncovalent Interactions, Excited States, and Transition Elements: Two New Functionals and Systematic Testing of Four M06-Class Functionals and 12 Other Functionals. *Theor. Chem. Acc.* **2008**, *120*, 215−241.
(43) Tomasi, J.; Mennucci, B.; Cammi, R. Quantum Mechanical Continuum Solvation Models. *Chem. Rev.* **2005**, *105*, 2999−3093.
(44) Čížek, J. On the Use of the Cluster Expansion and the Technique of Diagrams in Calculations of Correlation Effects in Atoms and Molecules. *Adv. Chem. Phys.* **1969**, *14*, 35−89.
(45) Purvis, G. D., III; Bartlett, R. J. A Full Coupled-Cluster Singles and Doubles Model: the Inclusion of Disconnected Triples. *J. Chem. Phys.* **1982**, *76*, 1910−1918.
(46) Halkier, A.; Helgaker, T.; Jørgensen, P.; Klopper, W.; Koch, H.; Olsen, J.; Wilson, A. K. Basis-Set Convergence in Correlated Calculations on Ne, N_2, and H_2O. *Chem. Phys. Lett.* **1998**, *286*, 243−252.
(47) Helgaker, T.; Klopper, W.; Koch, H.; Noga, J. Basis-Set Convergence of Correlated Calculations on Water. *J. Chem. Phys.* **1997**, *106*, 9639−9646.
(48) Dunning, T. H., Jr. Gaussian Basis Sets for Use in Correlated Molecular Calculations. I. The Atoms Boron through Neon and Hydrogen. *J. Chem. Phys.* **1989**, *90*, 1007−1023.
(49) Schlegel, H. B. Potential Energy Curves Using Unrestricted Møller-Plesset Perturbation Theory with Spin Annihilation. *J. Chem. Phys.* **1986**, *84*, 4530.
(50) Mayer, I. Spin-Projected EHF Method. IV. Comparison of Potential Curves Given by Different One-Electron Methods. *Adv. Quantum Chem.* **1978**, *14*, 29−38.
(51) Comeau, D. C.; Bartlett, R. J. The Equation-of-Motion Coupled-Cluster Method. Applications to Open- and Closed-Shell Reference States. *Chem. Phys. Lett.* **1993**, *207*, 414−423.
(52) Furche, F.; Ahlrichs, R. Adiabatic Time-Dependent Density Functional Methods for Excited State Properties. *J. Chem. Phys.* **2002**, *117*, 7433−7447.
(53) Wigner, E. On The Quantum Correction for Thermodynamic Equilibrium. *Phys. Rev.* **1932**, *40*, 749−759.
(54) Bonačić-Koutecký, V.; Mitrić, R. Theoretical Exploration of Ultrafast Dynamics in Atomic Clusters: Analysis and Control. *Chem. Rev.* **2005**, *105*, 11−66.
(55) Barbatti, M.; Ruckenbauer, M.; Plasser, F.; Pittner, J.; Granucci, G.; Persico, M.; Lischka, H. Newton-X: A Surface-Hopping Program for Nonadiabatic Molecular Dynamics. *Wiley Interdiscip. Rev. Comput. Mol. Sci.* **2014**, *4*, 26−33.
(56) Gilbert, R. G.; Smith, S. C. *Theory of Unimolecular and Recombination Reactions*; Blackwell Scientific Publications: Oxford, U.K., 1990; pp. 52−132.
(57) Zhu, L.; Hase, W. L. *Quantum Chemistry Program Exchange*; Indiana University: Bloomington, IN, 1994. ; Program no. QCPE 644
(58) Gregersen, J. A.; Tureček, F. Mass-Spectrometric and Computational Study of Tryptophan Radicals (Trp + H)• Produced by Collisional Electron Transfer to Protonated Tryptophan in the Gas Phase. *Phys. Chem. Chem. Phys.* **2010**, *12*, 13434−13447.
(59) Berendsen, H. J. C.; Postma, J. P. M.; van Gunsteren, W. F.; DiNola, A. R. H. J.; Haak, J. R. Molecular dynamics with coupling to an external bath. *J. Chem. Phys.* **1984**, *81*, 3684−3690.
(60) Stewart, J. J. P. Optimization of Parameters for Semi-Empirical Methods V: Modification of NDDO Approximations and Application to 70 Elements. *J. Mol. Model.* **2007**, *13*, 1173−1213.
(61) Řezáč, J.; Fanfrlík, J.; Salahub, D.; Hobza, P. Semiempirical Quantum Chemical PM6 Method Augmented by Dispersion and H-bonding Correction Terms Reliably Describes Various Types of Noncovalent Complexes. *J. Chem. Theory Comput.* **2009**, *5*, 1749−1760.
(62) Stewart, J. J. P. *MOPAC 16*. Stewart Computational Chemistry, Colorado Springs, CO (2016).
(63) Řezáč, J. Cuby: an Integrative Framework for Computational Chemistry. *J. Comput. Chem.* **2016**, *37*, 1230−1237.
(64) Řezáč, J.: *Cuby—ruby Framework for Computational Chemistry*; Version 4, http://cuby4.molecular.cz
(65) March, R. E.; Todd, J. F. J. *Quadrupole Ion Trap Mass Spectrometry*, 2nd Edition.; Wiley-Interscience: Hoboken, NJ, 2005. p. 123.
(66) Danell, R. M.; Danell, A. S.; Glish, G. L.; Vachet, R. W. The Use of Static Pressures of Heavy Gases within a Quadrupole Ion Trap. *J. Am. Soc. Mass Spectrom.* **2003**, *14*, 1099−1109.
(67) McLuckey, S. A.; Goeringer, D. E. Slow Heating Methods in Tandem Mass Spectrometry. *J. Mass Spectrom.* **1997**, *32*, 461−474.
(68) Pepin, R.; Tureček, F. Kinetic Ion Thermometers for Electron Transfer Dissociation. *J. Phys. Chem. B* **2015**, *119*, 2818−2826.
(69) Yates, B. F.; Bouma, W. J.; Radom, L. Distonic Radical Cations: Guidelines for the Assessment of Their Stability. *Tetrahedron* **1986**, *42*, 6225−6234.
(70) Hammerum, S. Distonic Radical Cations in Gaseous and Condensed Phase. *Mass Spectrom. Rev.* **1988**, *7*, 123−202.
(71) Vannier, L. A.; Yao, C.; Tureček, F. 2-Deoxyribose Radicals in the Gas Phase and Aqueous Solution. Transient Intermediates of Hydrogen Atom Abstraction from 2-Deoxyribofuranose. *Collect. Czech. Chem. Commum.* **2005**, *70*, 1769−1786.
(72) Dang, A.; Liu, Y.; Tureček, F. UV-Vis Action Spectroscopy of Guanine, 9-Methylguanine and Deoxyguanosine Cation Radicals in the Gas Phase. *J. Phys. Chem. A* **2019**, *123*, 3272−3284.

https://dx.doi.org/10.1021/acs.jpca.0c10293
J. Phys. Chem. A 2021, 125, 338−348